A Micromachined Freestanding Electrochemical Sensor for Measuring Dissolved Oxygen

Didi She and Mark G. Allen, *Fellow, IEEE*

***Abstract*— A freestanding, miniaturized electrochemical oxygen sensor for biomedical implantation has been microfabricated and characterized. The sensor is fabricated on a flexible and biocompatible polyimide substrate using lithographic techniques and singulated with an excimer laser. The sensor consists of a round-shaped planar sensing portion (diameter: 2.4 mm and thickness: 180 μm) and metal lines and contact pads for connection with external analytical tools. The sensing portion is comprised of three electrodes (working, counter, and reference electrodes), an electrolyte reservoir filled with liquid electrolyte, and a semipermeable membrane for oxygen introduction. The electrodes are patterned using a single layer of gold without the adhesion layer to eliminate any multilayer metallic structure in the sensing region. Both polydimethylsiloxane and fluorinated ethylene propylene semipermeable membranes are characterized. The fabricated sensor demonstrated an oxygen response of −14 nA/atm.% and good linearity (correlation coefficient exceeding 0.99). This device can potentially be incorporated into physiological applications, including monitoring oxygen tension in biomedical-related applications over semi-chronic time periods. [2019-0004]**

***Index Terms*— Electrochemical sensor, microfabrication, miniaturization, noble metal, three-electrode configuration.**

I. INTRODUCTION

ELECTROCHEMICAL sensors are one of the most widely used diagnostic tools in clinical analysis, environmental monitoring, and the food industry, due to their rapid response, low cost, and ease of applicability in the field. The ability to safely and reliably detect oxygen tension over semi-chronic time periods (e.g., weeks to months) is extremely desirable. The Clark cell is a well-established method for measuring dissolved oxygen concentration based on electrochemical principles [1]. The technology has been well-studied and sensors based on this method are commercially available. However, the sizes of the commercial sensors have precluded their use in clinical applications. For example, theoretical studies have shown that local oxygen tension appears to be an important factor in bone regenerative processes. The ability to acquire real-time measurements of oxygen tension within the regenerative niche in situ would significantly enhance the information available to tissue engineers to monitor and evaluate mechanisms of functional healing or lack thereof [2]. However, electrochemical oxygen sensors that are commercially available neither satisfy the size nor biocompatibility requirements needed for *in vivo* monitoring [3]. In addition, many commercial oxygen sensors incorporate hazardous chemicals such as lead or inorganic acids, rendering them less suitable for food industry or environmental monitoring. Development of a miniaturized, biocompatible and disposable electrochemical oxygen sensor with long shelf and functional lifetime that does not contain these materials may be desirable for both clinical and environmental applications.

An electrochemical oxygen sensor comprises three elements: electrodes, liquid electrolyte, and an oxygen permeable membrane. When a voltage is applied between electrodes, the current generated by electrochemical redox reactions is proportional to the dissolved oxygen content that has diffused through the oxygen permeable membrane into the liquid electrolyte. For the realization of a miniaturized electrochemical sensor, a significant challenge lies in the fabrication of a set of reliable and durable electrodes, as well as the incorporation of a miniaturized reservoir to store the liquid electrolyte in the electrochemical cell.

There have previously been attempts to fabricate electrochemical oxygen sensors using microfabrication technologies. A typical example is the thin-film Ag/AgCl structure demonstrated by Suzuki *et al.* [4]. In this structure the entire surface of the thin-film pattern was covered with a hydrophobic polymer layer leaving slits at the edges of the pattern, rendering the AgCl layer less susceptible to deterioration during sensor operation. However, the open circuit potential of the Ag/AgCl element was maintained for only 3–5 days after injection of electrolyte, after which a rapid negative shift of potential was observed. The stability and durability of the electrodes still are limiting factors to the shelf life and functional lifetime of the sensor [5]–[11]. Noble metals, such as platinum and gold, have also been used as the electrodes. Park *et al.* [12] demonstrated a reservoir-type oxygen sensor featuring gold electrodes; a lifetime test showed that the response current abruptly changed over 20% after 10.6 hours. Wu *et al.* [13] reported a Clark sensor chip consisting of a glass substrate and platinum electrodes, and the results showed that the difference of the relative responses from the first response increased 10% after 50 minutes. The fluctuations in sensor response were

---

Manuscript received January 6, 2019; revised February 18, 2019; accepted February 23, 2019. Date of publication March 22, 2019; date of current version May 31, 2019. This work was supported in part by the National Institute of Health under Grant R21-AR066322, in part by the National Science Foundation under Grant CMMI-1362652, and in part by the NSF National Nanotechnology Coordinated Infrastructure Program under Grant 15-42153. Subject Editor Y. Zohar. *(Corresponding author: Didi She.)*

The authors are with the School of Engineering and Applied Science, University of Pennsylvania, Philadelphia, PA 19104 USA (e-mail: didishe@seas.upenn.edu; mallen@seas.upenn.edu).

Color versions of one or more of the figures in this paper are available online at http://ieeexplore.ieee.org.

Digital Object Identifier 10.1109/JMEMS.2019.2903457

suspected to be attributable to the change in surface status of the electrodes, and the shift in potential of the reference electrodes, but little has been further explored to improve their performance in stability and lifetime.

Another challenge in the design and fabrication of a miniature electrochemical oxygen sensor is the integration of the electrodes with an electrolyte and oxygen-permeable membrane system that supports compact packaging. To form a compartment for the internal electrolyte, previous studies mainly attached a separate electrolyte reservoir to a chip to form a microfluidic system [9], [14], [15]. Although this process provides a simple and reproducible fabrication process, the overall dimension of the sensor is increased. In addition, for applications such as implantable and wearable biomedical sensors, good flexibility is required to reduce discomfort. However, the reported miniature electrochemical oxygen sensors generally lack flexibility and substrate and electrode failures due to mechanical stress have been observed. Further, most Clark-type sensors developed in the lab are characterized using a commercially available laboratory potentiostat, which is usually a bulky system and further compromises the sensor's portability for clinical use [9]–[22].

In an attempt to develop a miniaturized electrochemical sensor with good response to oxygen, various materials, structures and dimensions, as suggested by reported literature were evaluated on the basis of sensor performance, and designs that could optimize their use for electrochemical oxygen sensors were investigated. This study presents the development of a MEMS-based electrochemical sensor for monitoring of dissolved oxygen across a range of physiologically relevant concentrations. Specifically, this design comprises an oxygen permeable membrane, a freestanding electrolyte reservoir and a set of gold electrodes. Two oxygen permeable polymers, polydimethylsiloxane (PDMS) and fluorinated ethylene propylene (FEP), were investigated. The overall dimension of the sensor is 2.5 mm × 6 mm × 0.3 mm. Acustomized potentiostat platform with nanoampere current measurement and wireless data transmission capability was developed. Depending on the size constraints of the anatomical space under investigation, transceiver and circuitry components could be packaged within a single device or wires could be routed to a remote transceiver pack mounted either intraperitoneally or subcutaneously in implantable applications.

Earlier works on microfabricated electrochemical oxygen sensor mainly focused on Ag/AgCl or platinum reference electrodes, while few, if any, aqueous-based three-gold-electrode freestanding oxygen sensor has been reported. This work provides an easy way to fabricate a freestanding, disposable gold-based oxygen sensor with improved flexibility. The gold electrodes are single-layer noble metallic structures without any consumable parts, which avoids many of the problems with dimension and performance seen with existing miniature electrochemical oxygen sensors. In addition, a new fabrication process is developed to integrate the FEP membrane. The devices exhibit good response and prolonged shelf and functional lifetime. Further, the sensor can be bent in the non-functional region without alternating the redox current, demonstrating good flexibility for applications involving mechanical loading. For instance, the sensor can be integrated with the structural implant to monitor oxygen tension during bone regeneration in a rodent femoral defect model [2]. The contact pad region can be anchored to the bone fixation plate, while the oxygen-sensitive part of the sensor is inserted into the bone defect. In this application, substrate flexibility of the planar sensor is important for accommodating the slight vertical displacement of the contact pad region and bending in the middle of the sensor induced by force loading at the structural implant.

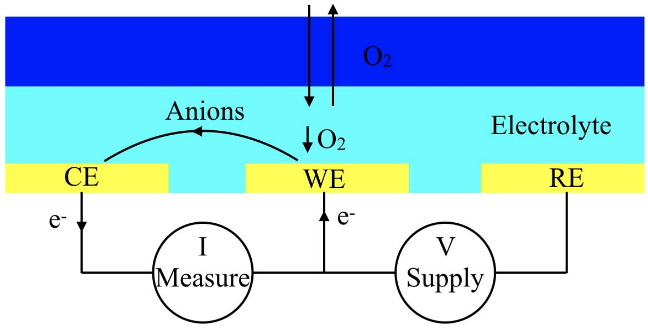

Fig. 1. Operation of an electrochemical oxygen sensor. A potentiostat is used as the external circuit to apply a voltage and measure current. When a negative potential is applied from the circuit across the working and reference electrodes, oxygen in contact with the working electrode is reduced, and thus generating an electric current.

II. EXPERIMENTAL

A. Working Principle

The basic principle of electrochemical oxygen sensors is the measurement of the current-potential relationship in an electrochemical cell, operated by measuring the electrical signal resulting from analyte reactions at the electrode. As shown in Fig. 1, the electrochemical oxygen sensor comprises three elements: electrodes, liquid electrolyte, and an oxygen permeable membrane. Oxygen molecules that come in contact with the sensor first permeate through a membrane, which also serves as protection against non-target molecules. The oxygen molecules then diffuse through the inner electrolyte to reach the surface of the working electrode (also known as the sensing electrode). There the molecules are reduced, consequently consuming electrons, and thus generating an electric current. The reduction reaction is a multielectron reaction often associated with the formation of reaction intermediates. Several reaction mechanisms have been suggested [25]:

(i) A direct four electron reduction to H_2O:

$$O_2 + 4H^+ + 4e^- \rightarrow 2H_2O \tag{1}$$

(ii) A two-electron pathway involving reduction to hydrogen peroxide:

$$O_2 + 2H^+ + 2e^- \rightarrow H_2O_2 \tag{2}$$

(iii) A four-electron process reduction that occurs in two steps:

$$O_2 + 2H^+ + 2e^- \rightarrow H_2O_2 \tag{3}$$
$$H_2O_2 + 2H^+ + 2e^- \rightarrow 2H_2O \tag{4}$$

The current is proportional to the rate of reaction at the sensing electrode, the potential of which is commonly regulated using the reference electrode. The reference electrode provides a constant potential and serves to maintain the voltage of the sensing electrode at desired values. The electrochemical cell is completed by the counter electrode which balances the reaction at the working electrode. The ionic current between the counter and sensing electrode is transported by the electrolyte inside the sensor body, whereas the external current path is provided by the potentiostat circuits.

B. Material Selection

Ag-AgCl/Cl^- is a self-contained electrochemical system, which makes it a good candidate as reference electrode for many industrial applications where the electrochemical potential must be accurately measured or controlled. Due to its stability and simplicity of fabrication, macroscopic Ag/AgCl structures are commonly used as the reference electrode in commercial oxygen sensors. A macroscale Ag/AgCl/KCl system can provide a stable reference potential for the reduction reaction on the cathode. In addition, silver can also serve as the anode, providing material for the oxidation reaction. However, reducing the dimensions of the silver and silver chloride for miniaturized sensors may cause complications in device operation [4]. Specifically, silver can be consumed by chloridization and silver chloride reacts with chloride ions (Cl^-) to form a soluble product in solutions with high Cl^- concentrations. At reduced size configurations, the electrochemical and chemical stability of silver and silver chloride becomes a limiting factor in shelf life or functional lifetime of the oxygen sensor. Second, the silver chloride thin film structure can be damaged under mechanical stress, which makes it less desirable for flexible substrates or applications involving mechanical loading.

A thin-film noble metal structure is another option for electrodes; this choice features inexpensive fabrication, as well as prolonged shelf and functional life. The inertness of the electrode material decreases the risk of electrode deterioration during measurement, which might lead to a large alteration of the electrolyte composition in a small, volume-constrained electrolyte chamber. In addition, an inert counter electrode can eliminate the consumption of anodic material, providing a relatively long-term functional lifetime. However, the potential of a pure metal electrode is not well defined and susceptible to instability. Drift in the reference electrode potential can cause quantitative errors in data collection beyond simple inaccuracies in the measured potential. Fortunately, this shortcoming can be overcome by using linear sweep voltammetry (LSV) for low frequency characterization, as discussed later in this study.

A three-electrode system built with a single metal, such as gold or platinum, is selected to satisfy all relevant design requirements. Although gold is less noble than platinum, it was experimentally observed that gold-based sensors demonstrated less drift than platinum-based sensors. This may be attributed to hydrogen absorption on the platinum electrodes, which causes a larger potential shift compared to gold throughout the measurement duration. The remaining, slight drift in reference potential can be overcome by using LSV for characterization. As a result, gold was selected as the material for all three electrodes.

The oxygen transport rate through the membrane is one of the most important factors that affects the response of the oxygen sensor. Polydimethylsiloxane (PDMS) has been widely used as the membrane material for its high oxygen permeability (i.e., 600 Barrer) [12]. Fluoropolymer is another good candidate for the oxygen-permeable membrane. Compared with PDMS [16], fluoropolymers have several advantages [12], [17], such as less absorption of small molecules and biomolecules, and less leaching of irrelevant molecules from the environment into the electrolyte in the reservoirs. The oxygen permeability of fluorinated ethylene propylene (FEP) is 5.9 Barrer [12], which is relatively high among fluoropolymers, rendering FEP another candidate for the membrane. Among the polymers, polyimide possesses high thermal and hydrolytic stability, excellent chemical resistance, excellent adhesion properties and good mechanical strength. Therefore, PDMS, FEP and commercial polyimide films (Kapton HN, Dupont) were chosen as the membrane material and device substrate, respectively; oxygen sensors based on these polymers are fabricated and characterized.

C. Design and Fabrication

Several electrode design issues are considered to improve device response and sensor stability. To achieve a sufficiently high output signal and, therefore, response, the sensor requires a sufficient working electrode area to support oxygen reduction. However, the dependence of the output current on cathode area is not a simple linear relationship. Previous studies have shown that the current is approximately proportional to the area of cathode electrode until it saturates at a threshold value, which primarily depends on the dimension of the electrolyte reservoir. Second, to ensure that the potential at the counter electrode is sufficiently low to eliminate oxidation of the electrode material, a high surface area ratio between the counter and working electrodes is required. Third, a sufficient reference electrode area is also desirable in order to maintain a stable reference voltage. In addition, the relative position of the three electrodes and the distance between them must also be considered. In most electrochemical systems, the reference electrode should be placed near to the working electrode to minimize Ohmic losses and to provide a uniform electric field. However, in the electrochemical oxygen sensor, it is better to separate the electrodes as much as possible to eliminate crosstalk between electrodes [23], [24].

The designed dimension of the oxygen sensor is 2.5 mm $\times$ 6 mm $\times$ 0.3 mm, with a slimmer neck in the middle, as later shown in Fig. 3.The connecting wires in the neck region are passivated to eliminate the redox reactions. Leaving out the connecting wires and solder pad region, the functional region of the sensor is 2.4 mm in diameter. The distance between the cathode surface and the gas permeable membrane is approximately 6 μm, providing an inner electrolyte system of 0.027 mm^3. Guided by other reported sensors [12], the cathode area for maximum signal saturation is set to approximately 0.2 mm^2. To minimize crosstalk between the electrodes, the electrode separation distance is 200 μm in the present work. Therefore, a reasonable surface area ratio of the working, reference, and counter electrodes is approximately 1:1:5, with a working electrode footprint that is 400 μm in diameter.

A thin layer (i.e., <20 nm thickness) of chromium is commonly used in microfabrication to improve the adhesion between electron-beam-evaporated gold and a base substrate. Although chromium (Cr) might improve the adhesion of the device electrodes to the polyimide substrate [26]–[28], a multilayer metallic structure may also introduce complications to the electrochemical system, potentially resulting in abnormal behavior and/or decreased responseor stability of the sensor [4]. In such systems, the exposed edge of Cr could lead to a mixed potential on the reference electrode. Also, Cr has a negative redox potential relative to gold, potentially leading to more facile oxidation and subsequent deterioration of the sensor electrode. Finally, dissolved chromium ions might migrate to the cathode; and their reduction at the working electrode could cause an increase in current not reflective of oxygen concentration. Hence, a chromium adhesion layer extending into the sensor/electrolyte region was undesirable in the fabrication of an electrochemical oxygen sensor. However, complete removal of the adhesion layer is problematic. Without such a layer it was experimentally observed that the working and counter electrodes wrinkle and then physically deform after a very short duration of functionality; further, the absence of an adhesion layer in the pad region rendered subsequent processing more difficult (e.g., delamination of electroplated copper in the contact pads during soldering).

To overcome these difficulties, we developed an electrode fabrication scheme that incorporates a partial adhesion layer and a mesh electrode morphology as shown in Fig. 2. An adhesion layer of chromium is patterned only in the contact pad region, where copper will be electroplated. The mesh structure consists of 20-μm-diameter holes arranged in a radial array. The first thin layer of Au/Cr was deposited onto the polyimide substrate by electron-beam evaporation and lithographically patterned by lift-off, followed by the deposition and patterning of a second, thicker Au layer. To achieve the mesh design, the working and counter electrodes were patterned with an excimer laser, whose micromachining conditions were optimized to ablate the thin film metal without damaging the underlying polymeric substrate. It was experimentally observed that the electrode mesh morphology reduced the deformation and delamination problem of the electrodes, and the Cr layer greatly improved the adhesion between the metallic contact pad and polyimide substrate and increased tolerance to stress induced in soldering and encapsulation.

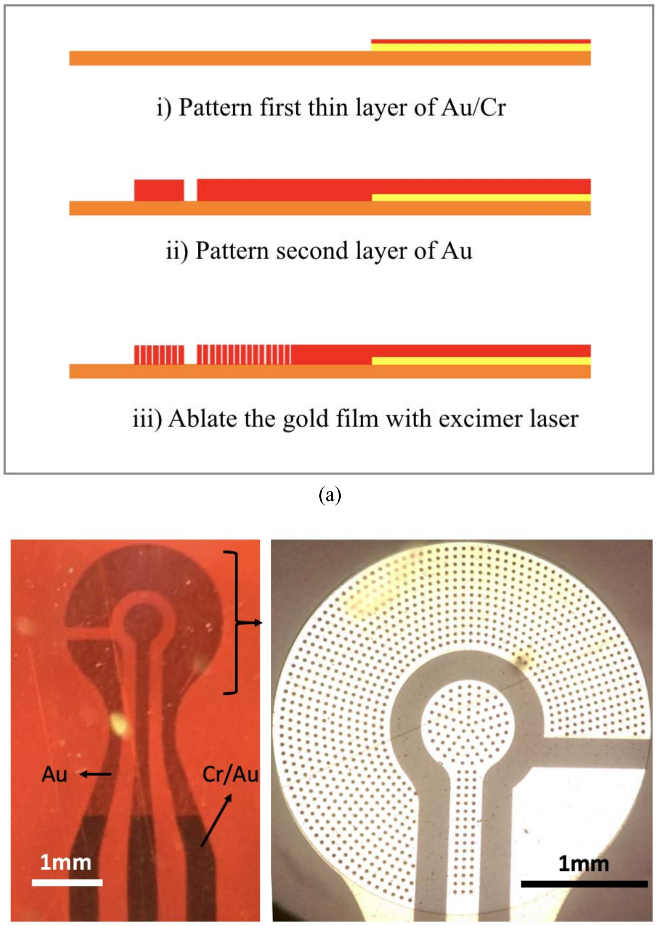

(a)

(b) (c)

Fig. 2. (a) Fabrication scheme of sensor electrode on polyimide substrate; (b) optical images of sensor electrodes after step (ii) as seen from the backside. The Cr region can be seen through the translucent polyimide; (c) Sensor electrode top view after step (iii).

A schematic of the oxygen sensor fabrication process incorporating PDMS as the oxygen-permeable membrane is illustrated in Fig. 3. The gold electrodes were patterned onto the polyimide substrate as described above. Five small pores (60 μm in diameter) were formed through the polyimide film in between the working and counter electrodes using an excimer laser to enable subsequent injection of the inner electrolyte prior to activation of the sensor. A 3 μm thick SU-8 layer was then patterned to passivate the gold leads. Aphotoresist (MicroChem SPR-220 7.0)pattern was used as a mold for the electrodeposition of copper on the contact pads (6 μm thickness). The inner electrolyte chamber was patterned using PVA, a water-soluble polymer with low solubility in organic solvents. The negative image of the chamber was patterned by 9-μm-thick SPR-220 7.0(MicroChem) and 20-μm-thick PVA (33 wt.%) was spin-cast onto the substrate and dried. The sample was treated by oxygen plasma to remove any PVA coating the edges of the photoresist and, subsequently, sonicated in acetone to dissolve the photoresist and achieve a micropatterned water-soluble mold. PDMS was then spin-coated and cured at 70 °C to form the electrolyte reservoir with a 15 μm thick oxygen permeable membrane. The copper contact pads were exposed by using tape to lift off the PDMS in that area. Finally, sensors were singulated with an excimer laser, soldering was performed for electrical connection, and exposed contacts were encapsulated with a UV curable encapsulant(Dymax 3401). An optical image of a fabricated senor is shown in Fig. 4.

The fabrication process of electrolyte reservoir featuring FEP membrane is shown in Fig. 5. The steps through the

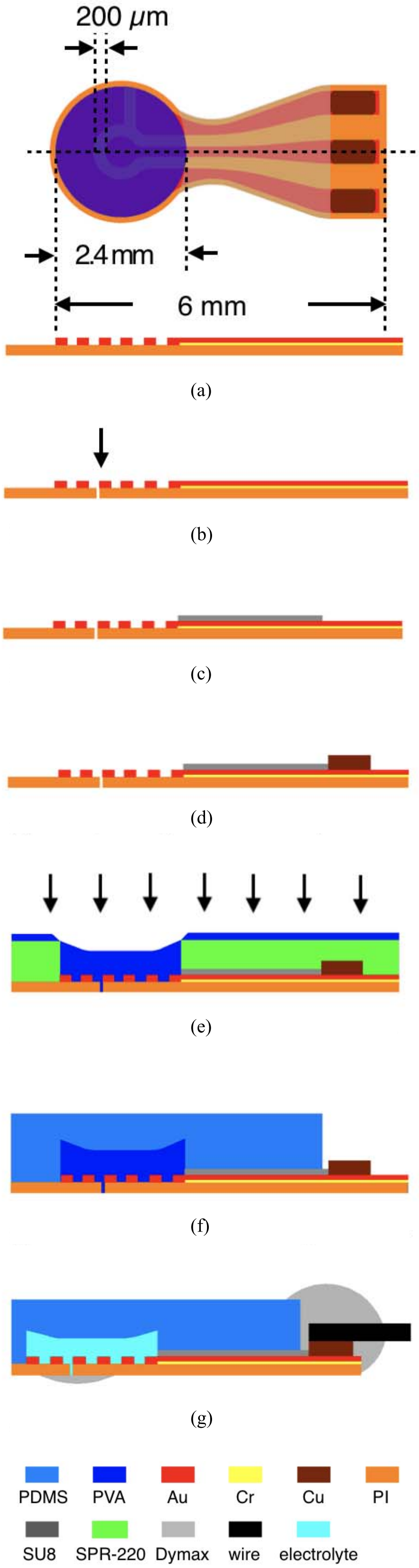

Fig. 3. Fabrication process of the oxygen sensor incorporating PDMS as the oxygen-permeable membrane. (a) Electrodes formed as described in Fig. 2. (b) Pores formed through polyimide substrate. (c) Passivate the gold leads using SU-8. (d) Electroplate copper on the contact pad. (e) Pattern inner electrolyte chamber using PVA. (f) Pattern PDMS to form the electrolyte reservoir. (g) Cut the sensor and form electrical connection.

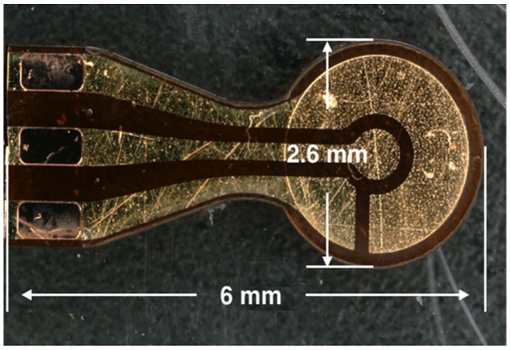

Fig. 4. Optical image of the fabricated sensor.

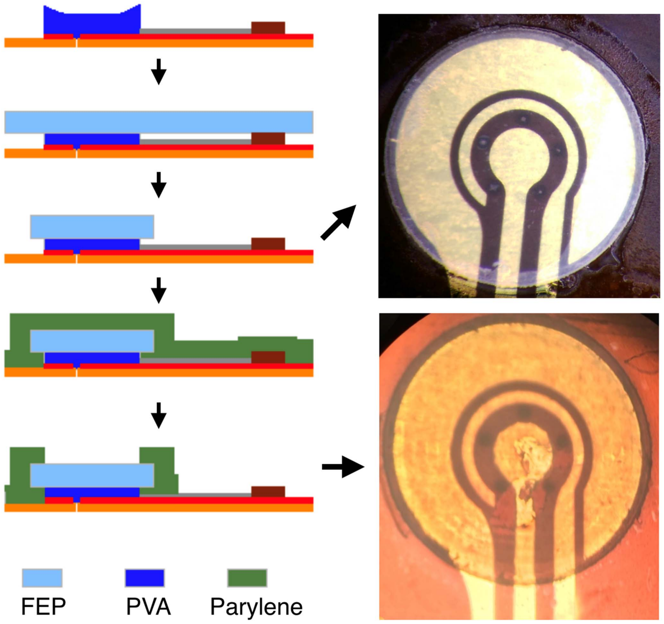

Fig. 5. The fabrication process of electrolyte reservoir featuring FEP membrane.

patterning of electrodes and electrolyte reservoir are the same as demonstrated in Fig. 3, from step (a) to step (e). After the chamber is patterned with a sacrificial PVA structure, a 12 μm thick FEP membrane was laminated onto the top and cut with excimer laser to the size of the foot print of the electrolyte chamber. Subsequently, 10 μm thick Parylene was deposited to seal the FEP film to the substrate. An excimer laser was again used to etch down Parylene to expose the FEP film and copper pad area, and the micromachining conditions were optimized to ablate the Parylene film without damaging the underlying oxygen-permeable membrane. Specifically, the fluence used to ablate Paryleneis in the range 0.4–0.6 J/cm^2 to maximize the removal rate of Parylene without impacting the substrate [29]. Sensors were subsequently cut, wired and encapsulated as discussed in Fig. 3.

The inner electrolyte comprises a 0.1 M NaCl solution, as it is the major ionic content of many physiological environments [30]. In order to fill the chamber with electrolyte, the sample was immersed in 0.1 M NaCl for 12 hours to allow the electrolyte to infiltrate through the laser-ablated pores on the back side of the sensor and to dissolve the remaining PVA. It is assumed that the remaining PVA is diluted during this process to a negligible concentration. The pores in the sensor substrate are sealed from the backside. The sensor was placed with the top side faced downward on a surface wetted with 0.1 M NaCl solution to prevent evaporation of inner electrolyte, and a thin layer of Dymax 3401 was applied to the laser-ablated pores on the back side. UV light was applied to cure the Dymax 3401 and therefore seal the electrolyte reservoir. The membrane is 12 μm in thickness and separated from the electrodes by a 6-μm-thick inner electrolyte cell containing a 0.1 M NaCl solution.

D. Customized Potentiostat

A customized potentiostatis developed to interface with the sensor and provide wireless data transmission capability. The analog circuitry contains a digital-to-analog converter (DAC) and two operational amplifiers (op-amps) with negative feedback for generating voltage waveforms and quantifying current at sufficient precision. The objective of the circuit is to provide a regulated voltage between the WE and the RE and to deliver an output voltage proportional to the sensor output current (produced by any electrochemical reactions on the electrodes). The voltage between the WE and RE are controlled and maintained by the DAC and op-amps, and can be modulated as a function of time in a pattern dependent on the type of required experiment, e.g., in this case, a linear change for linear LSV. The op-amp controlling the voltage of the WE also functions as a trans impedance amplifier that converts the current from the inverting input into a voltage, which can be calculated by:

$$V_{out} = V_W - I \bullet R \tag{5}$$

V_{out} represent output voltage of the transimpedance amplifier. V_W,I, R denote the WE voltage, output current of the sensor, and feedback resistance of the trans impedance amplifier, respectively. When a negative potential is applied between WE and RE, the oxygen reduction occurs on the anode surface, and positive charges are generated in the sensor anode. Current flowing out of the WE feeds into the trans impedance amplifier and, in this manner, the output voltage is proportional to the charges generated in the oxygen reduction reaction. The CE is connected to the output of an op-amp, which will source adequate current to balance the current required by the WE. We employed TI LMV342IDGKR op-amps in the customized potentiostat because they feature very low offset voltage and input bias current and are low power. Specifically, these amplifiers have an input bias current of 1pA and an input bias voltage of 0.25 mV, which render it capable of regulating electrode voltage with millivolt precision and measuring electrode current with nanoamp precision. Output voltage of the transimpedance amplifier is fed into a MSP430 (TI CC430), which performs analog-to-digital (ADC) conversion, data storage and wireless transmission to a remote-control board. A commercial quarter wave antenna (433 MHz) and matching network were included to enhance the transmission intensity.

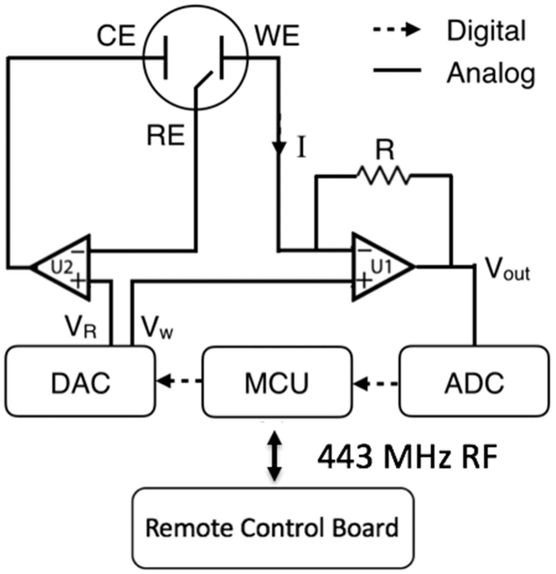

Fig. 6. Circuit schematic of the customized potentiostat connected to a three-electrode oxygen sensor.

III. RESULTS

A. Response Tests

Benchtop electrochemical testing of the electrochemical sensor was performed in a 0.1 M NaCl solution, where the oxygen concentration was tuned to the physiological range(i.e., 0 – 8.6mg/L at 25 °C and sea level) and calibrated to a commercial O_2 probe (Microx TX3, PreSens). Various O_2 concentrations were achieved in the solution by the addition of sodium sulfite (Na_2SO_3) in quantities sufficient to consume the excess oxygen due to a chemical reaction of oxygen with Na_2SO_3. Specifically, sulfite reacts with and consumes dissolved oxygen to produce sulfate, thus decreasing oxygen concentration in aqueous solutions [12]. Upon consumption of the sulfite, over time and in ambient conditions oxygen is naturally reintroduced into the solution; this gradual increase in oxygen concentration is monitored both by the commercial O_2 probe and by this electrochemical sensor and compared. Performance of the device was evaluated by LSV using a commercial potentiostat (Reference 600, Gamry). The bias potential between the working and reference electrodes was swept at a rate of −5 mV/s until the sensor reached the diffusion-limited regime. Fig. 7 shows the testing result of an oxygen sensor with a PDMS membrane thickness of 12 μm. The limiting current was identified as the intersection of the reaction-limited region and diffusion-limited region of the I–V curve (i.e., the circular markers in Fig. 7(a)). The corresponding calibration curve for the fabricated electrochemical oxygen sensor is shown in Fig. 7(b), where the current measurement is cross-referenced to the oxygen measurement from the commercial oxygen probe. The corresponding current of the reaction-limited region shifts towards more negative potentials as the oxygen concentration increases. As discussed earlier, while the durability of the gold reference electrode is superior to a simple thin-film Ag/AgCl pair, the potential exhibits

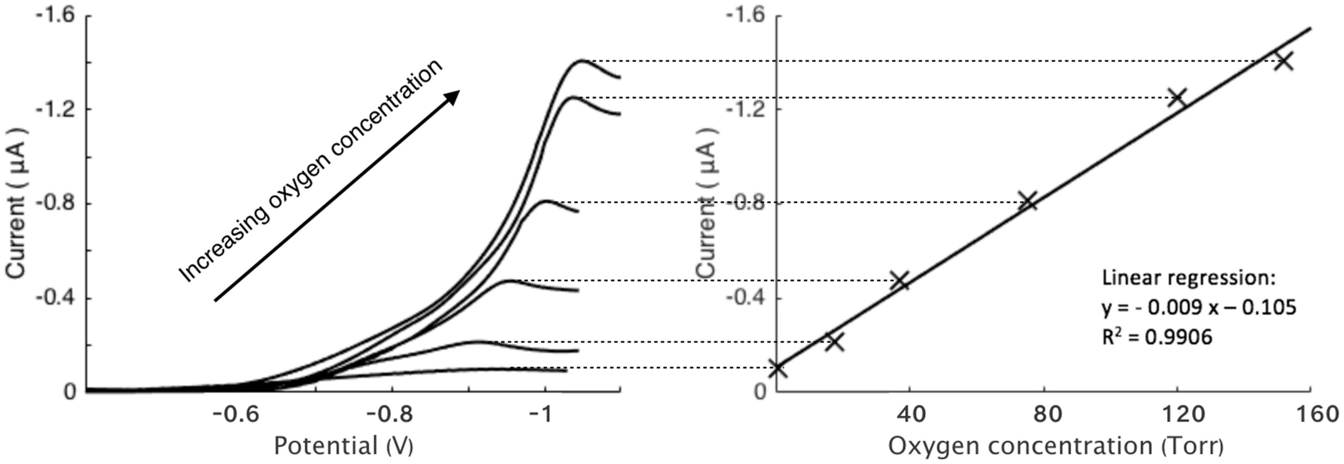

(a) (b)

Fig. 7. Electrical response of the fabricated electrochemical sensor. (a) Linear sweep voltammogram for a sensor tested within oxygen concentrations of 0.5%, 11%, 23%, 47%, 75%, 95% with respect to atmospheric oxygen. (b) The diffusion-limited-current/calibrated-O_2-concentration relationship. The sensor demonstrated linearity across a range of physiologically relevant concentrations.

more fluctuations—a shortcoming that can be overcome by using LSV to find the limiting current region. Specifically, the gold reference potential is drifting to more positive values during measurement, which leads to an increased potential difference between working electrode and reference electrode. Although the appearance of redox peak is shifting in the I–V curve, the absolute reduction potential might not be altered as greatly. Therefore, the plateau current still reflexes the oxygen tension under test. The fabricated sensor demonstrated an oxygen response of approximately −14 nA/atm.% and excellent linearity; linear regression yielded a correlation coefficient of 0.9906.

Bend test was performed to evaluate the resistance to mechanical failure of the sensor. Two plates were used to anchor the contact pad region and functional region, respectively, and the middle part of the sensor is bent to a specific angle by moving one plate to form an inside radius. The sensitivity of the sensor remained unchanged at a bending angle of 30 degrees in the middle part, demonstrating good flexibility for applications involving mechanical loading.

Sensors with different oxygen permeable membranes are compared in Fig. 8. The responses of the PDMS based sensors lie in a range from −9nA/atm.% to −14nA/atm.%. This variation was suspected to be introduced by the uniformity and consistency problem in the oxygen plasma treatment of the PVA sacrificial structure, which might lead to a variation in the size of the electrolyte reservoir. FEP based sensors have response between −1.8 nA/atm.% to −2.2 nA/atm.%, which was expected since FEP has lower oxygen permeability. Due to the variation in response, each sensor should be calibrated after infiltration of inner electrolyte. Sensors can be stored in solution for months prior to usage, since the sensor has no consumable parts, and the unbiased interior components show excellent stability with time.

Biological studies are usually conducted at body temperature (37 °C), while environmental monitoring tests are mostly taken at room temperature (20 °C). To determine the sensor performance at different temperature range, the sensor was characterized in 0.1 M NaCl solution at room temperature and body temperature, respectively. Fig. 9 shows the calibration curve of a sensor in 0.1 M NaCl at 20 °C and 37 °C. The sensor demonstrated an oxygen sensitivity of approximately −14.5 nA/atm.% at 20 °C, and approximately −17.5 nA/atm.% at 37 °C. This indicates that the sensitivity of the sensor changes over temperature at a rate of approximately 0.18 nA/atm.% °C.

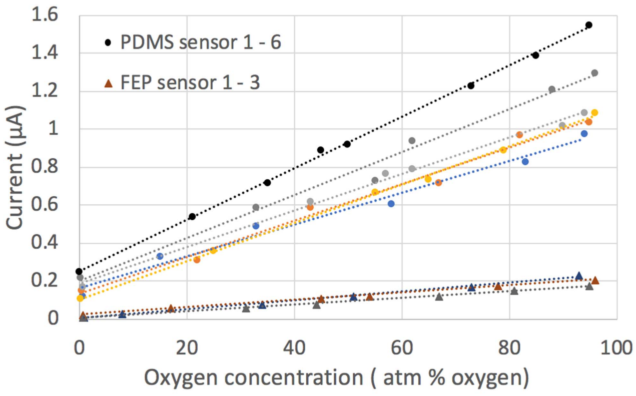

Fig. 8. Response characterization of the fabricated sensor with different oxygen permeable membranes.

B. Stability Tests

Oxygen sensors with a 12 μm thick PDMS membrane were utilized to analyze the stability performance. The test medium was a 0.1 M NaCl solution saturated with oxygen. LSV tests were performed periodically every hour at room temperature for a total of approximately two days, and three sets of response tests were performed (i.e., at the beginning, middle and end of the stability test). As shown in Fig. 10, the output current remained stable over the duration of 58 tests including the response tests. The sensor demonstrated similar

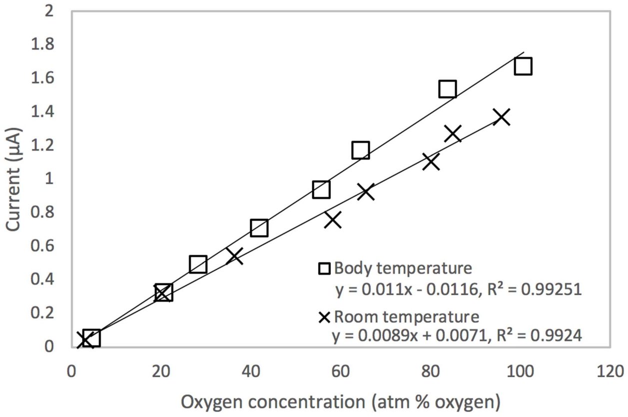

Fig. 9. Response characterization of the fabricated sensor at 20 °C and 37 °C.

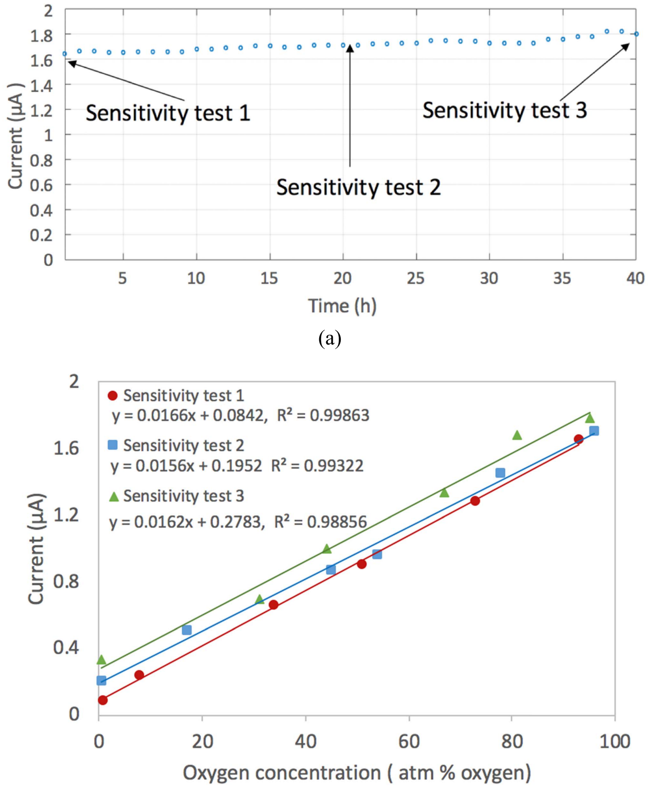

(a)

(b)

Fig. 10. (a) The stability results of the fabricated electrochemical oxygen sensor at room temperature by measuring the diffusion-limited reduction currents at a full-oxygen state 40 times sequentially. (b) The sensitivity results of 3 sets of tests.

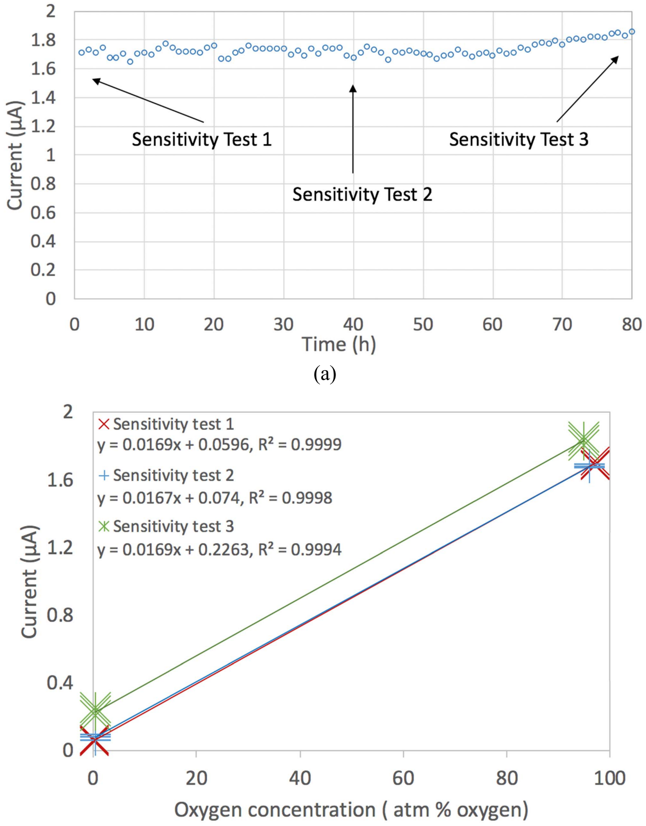

(a)

(b)

Fig. 11. (a) The stability results of the fabricated electrochemical oxygen sensor at 37 °C by measuring the diffusion-limited reduction currents at a full-oxygen state 80 times sequentially. (b) The sensitivity results of 3 sets of tests.

response at the beginning, middle and end of the stability test. The same tests were performed at body temperature for a total of 80 hours, and the response change over time were also evaluated. The solution under test was incubated in heated water and maintained at 37 °C. As shown in Fig. 11, the fluctuation in current at body temperature is slightly larger than at room temperature. This might be caused by slight temperature fluctuation of the water bath. The response test at both body temperature and room temperature showed relatively consistent slope, while the intercept increased over time. This indicates that the current shift during the tests is attributed to the increase of residual current.

i

C. Lifetime Tests

0.1M NaCl solution was used to evaluate the lifetime of the sensor at room temperature. Fig. 12 shows the life time characterization of the sensor at 20 °C obtained by cross-referencing to a commercial oxygen sensor. Measurements were performed periodically by LSV every hour until device failure. The inset shows the diffusion-limited reduction currents of the first 50 measurements cross referenced to the commercial sensor. The overall linearity of the 50 tests were obtained with a correlation coefficient of 0.99. An increasing current drift was observed after 140 tests. It is speculated that the deterioration in performance of the sensor is attributed to slow physical degradation of the metal film when currents flow through the electrodes. Fig. 13 shows testing results at full-state oxygen from custom sensor over 2 weeks, and the insets show simple sensitivity results at day 1 and day 14, respectively. The measured currents lied with in 1.56 ± 0.06 μA with a standard deviation of 0.04 except for day 9 and day 10, which have a high probability of being outliers, based on student's t-distribution. The large current change in day 9 and day 10 is suspected to originate from ambient

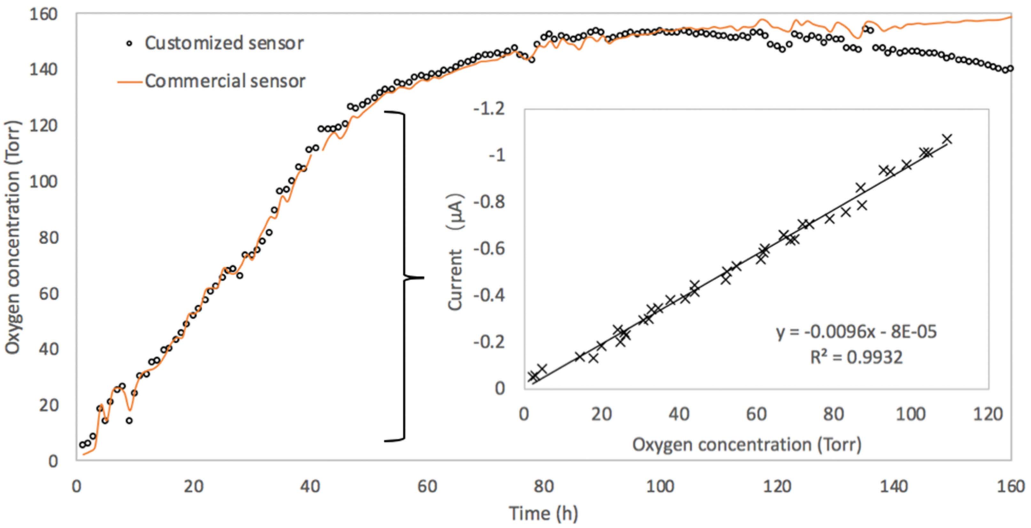

Fig. 12. Life time characterization of the fabricated oxygen sensor at room temperature. Data obtained from customized sensor (black circles) are cross-referenced to a commercial oxygen sensor (orange line).

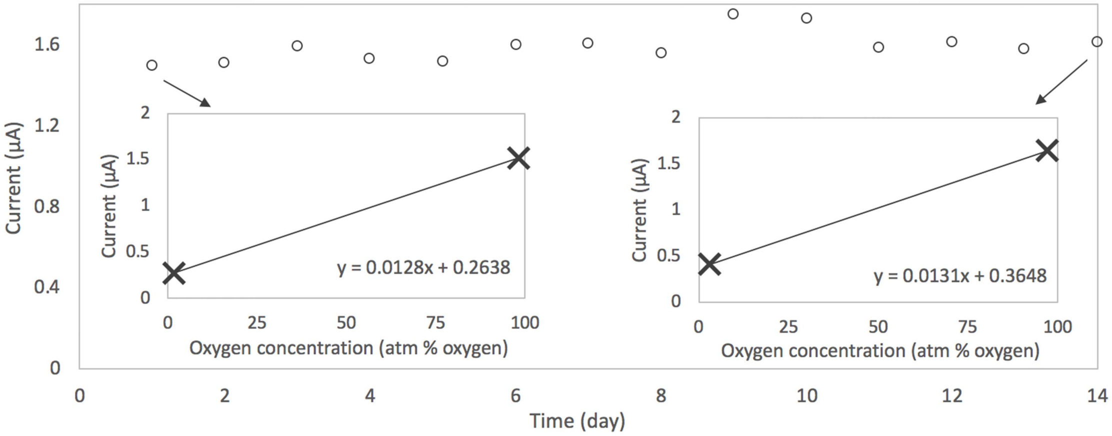

Fig. 13. Life time characterization of the fabricated oxygen sensor at room temperature by measuring the diffusion-limited reduction currents at a full-oxygen state over 2 weeks. The insets showed simple test results of the sensitivity in day 1 and day 14. Data obtained from customized sensor at oxygen-depleted state and full-oxygen state is cross-referenced to a commercial oxygen probe.

environmental change (e.g. temperature, convection), as the sensor sensitivity is not largely altered in 14 days.

As we discussed earlier, sensors can be stored in solution for months without alteration in sensitivity, since the sensor has no consumable parts, and the unbiased interior components have excellent stability with time. The sensors can potentially support testing for 140 days if one test is performed each day. In many biomedical applications, oxygen concentration is expected to change slowly, thus, sparse time point measurements may be satisfactory for biological research or for clinical use. The results suggested that the oxygen sensor is sufficient for monitoring oxygen tension in situ over semi chronic time periods (e.g., weeks to months)at physiological oxygen magnitudes.

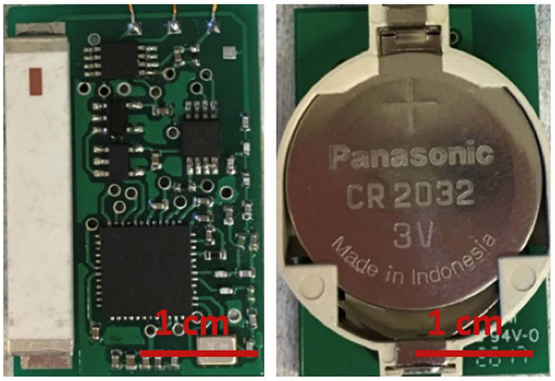

(a) (b)

Fig. 14. (a) Front and (b) back side of the wirelessly-controlled potentiostat circuit board. The overall dimension of the PCB board is 2 cm × 3 cm × 8 mm.

D. Customized Potentiostat

An optical image of the wirelessly controlled, customized potentiostat is shown in Figure 14. The dimension of the printed circuit board (PCB) is 30 mm × 20 mm × 8 mm. A CR 2032 battery holder was soldered on the backside of the board for onboard power supply. Fig. 15 shows the results of the end-to-end testing of the oxygen sensor connected to customized potentiostat. The I–V curve demonstrates a clear plateau for

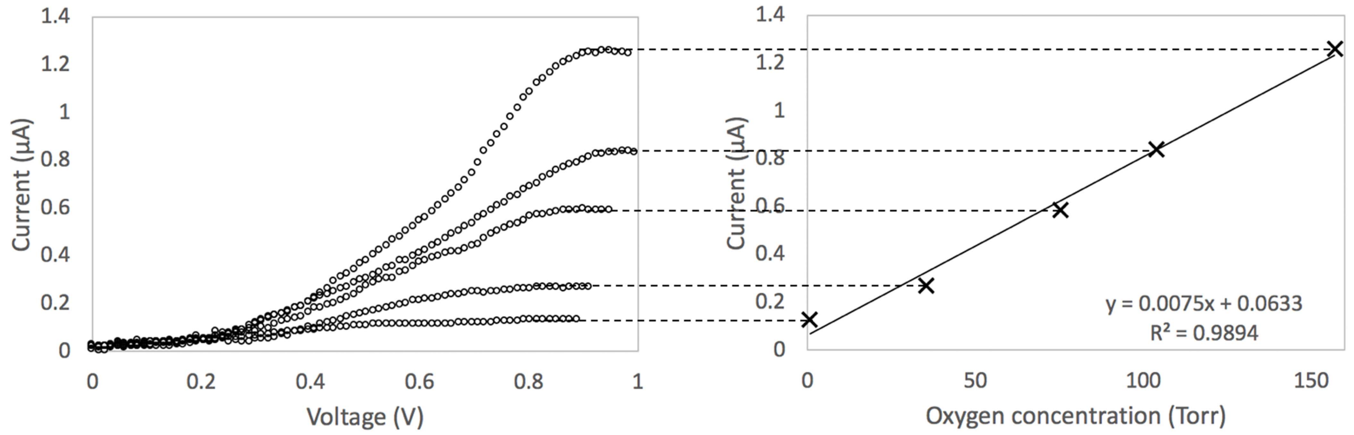

(a) (b)

Fig. 15. End to end testing and calibration of the oxygen sensing system. (a) LSV data obtained from customized potentiostat. (b) Corresponding current measured from the full system calibrated to a commercial oxygen sensor.

extracting the corresponded limiting reduction current at each oxygen concentration. The result is directly cross-referenced to the oxygen measurement from the commercial probe. This oxygen sensing system demonstrated an oxygen sensitivity of approximately 13 nA/atm.% and excellent linearity, confirming that the customized potentiostat can maintain accuracy sufficient for *in vivo* applications.

IV. CONCLUSIONS

Microfabricated Clark-type electrochemical oxygen sensors with integral electrochemical chambers were designed and fabricated, and their performance was examined. Features of the presented design include a freestanding and miniature structure. Two oxygen-permeable membrane materials were explored and their responses were compared. In order to maintain a stable reference potential during a long period of shelf and functional time, an inert gold electrode without adhesion layer was fabricated, and the remaining, slight drift in reference potential was overcome by using LSV for characterization. This design features fabrication of reliable and durable electrodes and easy integration of a miniaturized reservoir, thus providing a simplified strategy to fabricate freestanding, miniaturized oxygen sensors with a long shelf life and desirable functional life span.

ACKNOWLEDGMENT

Microfabrication was carried out at the Singh Center for Nanotechnology.

REFERENCES

[1] N. Akmal and J. Lauer, "Electrochemical oxygen sensors: Principles and applications," *Polym. Sensors*, vol. 690, pp. 149–160, Jan. 1998.

[2] B. S. Klosterhoff *et al.*, "Implantable sensors for regenerative medicine," *J. Biomech. Eng.*, vol. 139, no. 2, 2017, Art. no. 021009.

[3] D. She, M. Tsang, and M. Allen, "Biodegradable batteries with immobilized electrolyte for transient MEMS," *Biomed. Microdevices*, vol. 21, no. 1, p. 17, 2019.

[4] H. Suzuki, A. Hiratsuka, S. Sasaki, and I. Karube, "Problems associated with the thin-film Ag/AgCl reference electrode and a novel structure with improved durability," *Sens. Actuators B, Chem.*, vol. 46, no. 2, pp. 104–113, 1998.

[5] H. Suzuki, T. Hirakawa, S. Sasaki, and I. Karube, "An integrated module for sensing pO_2, pCO_2, and pH," *Anal. Chim. Acta*, vol. 405, nos. 1–2, pp. 57–65, 2000.

[6] H. Suzuki, T. Hirakawa, I. Watanabe, and Y. Kikuchi, "Determination of blood pO_2 using a micromachined clark-type oxygen electrode," *Anal. Chim. Acta*, vol. 431, no. 2, pp. 249–259, 2001.

[7] H. Suzuki, "Microfabrication of chemical sensors and biosensors for environmental monitoring," *Mater. Sci. Eng., C*, vol. 12, nos. 1–2, pp. 55–61, 2000.

[8] H. Suzuki, H. Ozawa, S. Sasaki, and I. Karube, "A novel thin-film Ag/AgCl anode structure for microfabricated Clark-type oxygen electrodes," *Sens. Actuators B, Chem.*, vol. 53, no. 3, pp. 140–146, 1998.

[9] H. Suzuki, H. Arakawa, and I. Karube, "Fabrication of a sensing module using micromachined biosensors," *Biosensors Bioelectron.*, vol. 16, nos. 9–12, pp. 725–733, 2001.

[10] C.-C. Wu, H.-N. Luk, Y.-T. T. Lin, and C.-Y. Yuan, "A Clark-type oxygen chip for *in situ* estimation of the respiratory activity of adhering cells," *Talanta*, vol. 81, nos. 1–2, pp. 228–234, 2010.

[11] M. Wittkampf, G.-C. Chemnitius, K. Cammann, M. Rospert, and W. Mokwa, "Silicon thin film sensor for measurement of dissolved oxygen," *Sens. Actuators B, Chem.*, vol. 43, nos. 1–3, pp. 40–44, 1997.

[12] J. Park, Y. K. Pak, and J. J. Pak, "A microfabricated reservoir-type oxygen sensor for measuring the real-time cellular oxygen consumption rate at various conditions," *Sens. Actuators B, Chem.*, vol. 147, no. 1, pp. 263–269, 2010.

[13] C.-C. Wu, T. Yasukawa, H. Shiku, and T. Matsue, "Fabrication of miniature Clark oxygen sensor integrated with microstructure," *Sens. Actuators B, Chem.*, vol. 110, no. 2, pp. 342–349, 2005.

[14] G. Koley, J. Liu, M. W. Nomani, M. Yim, X. Wen, and T.-Y. Hsia, "Miniaturized implantable pressure and oxygen sensors based on polydimethylsiloxane thin films," *Mater. Sci. Eng., C*, vol. 29, no. 3, pp. 685–690, 2009.

[15] S. Lee, B. L. Ibey, G. L. Coté, and M. V. Pishko, "Measurement of pH and dissolved oxygen within cell culture media using a hydrogel microarray sensor," *Sens. Actuators B, Chem.*, vol. 128, no. 2, pp. 388–398, 2008.

[16] M. W. Toepke and D. J. Beebe, "PDMS absorption of small molecules and consequences in microfluidic applications," *Lab Chip*, vol. 6, no. 12, pp. 1484–1486, 2006.

[17] H. Suzuki, A. Sugama, and N. Kojima, "Micromachined Clark oxygen electrode," *Sens. Actuators B, Chem.*, vol. 10, no. 2, pp. 91–98, 1993.

[18] R. Ramamoorthy, P. K. Dutta, and S. A. Akbar, "Oxygen sensors: Materials, methods, designs and applications," *J. Mater. Sci.*, vol. 38, no. 21, pp. 4271–4282, 2003.

[19] Z. Yang, S. Sasaki, I. Karube, and H. Suzuki, "Fabrication of oxygen electrode arrays and their incorporation into sensors for measuring biochemical oxygen demand," *Anal. Chim. Acta*, vol. 357, nos. 1–2, pp. 41–49, 1997.

[20] H. Suzuki, E. Tamiya, and I. Karube, "Fabrication of an oxygen electrode using semiconductor technology," *Anal. Chem.*, vol. 60, no. 10, pp. 1078–1080, 1993.

[21] A. Niazi and C. J. Anthony, "Development of oxygen sensor by integrating the low cost printed circuit board technology and solid electrolyte membrane," in *Proc. Int. Conf. Biomed. Eng. Syst.*, 2014, pp. 1–7.

[22] N. Yamazoe and N. Miura, "Solid-state electrochemical oxygen sensors for operation at room temperature," *TrAC Trends Anal. Chem.*, vol. 9, no. 5, pp. 170–175, 1990.

[23] D. J. Strike, A. Hengstenberg, M. Quinto, C. Kurzawa, M. Koudelka-Hep, and W. Schuhmann, "Localized visualization of chemical cross-talk in microsensor arrays by using scanning electrochemical microscopy," *Microchimica Acta*, vol. 131, nos. 1–2, pp. 47–55, 1999.

[24] M. S. Wilson, "Electrochemical immunosensors for the simultaneous detection of two tumor markers," *Anal. Chem.*, vol. 77, no. 5, pp. 1496–1502, 2005.

[25] R. Zeis, T. Lei, K. Sieradzki, J. Snyder, and J. Erlebacher, "Catalytic reduction of oxygen and hydrogen peroxide by nanoporous gold," *J. Catal.*, vol. 253, no. 1, pp. 132–138, 2008.

[26] S. Metz, R. Holzer, and P. Renaud, "Polyimide-based microfluidic devices," *Lab Chip*, vol. 1, 1, pp. 29–34, 2001.

[27] P. J. Rousche, D. S. Pellinen, D. P. Pivin, J. C. Williams, R. J. Vetter, and D. R. Kipke, "Flexible polyimide-based intracortical electrode arrays with bioactive capability," *IEEE Trans. Biomed. Eng.*, vol. 48, no. 3, pp. 361–371, Mar. 2001.

[28] S. P. Lacour *et al.*, "Flexible and stretchable micro-electrodes for *in vitro* and *in vivo* neural interfaces," *Med. Biol. Eng. Comput.*, vol. 48, no. 10, pp. 945–954, 2010.

[29] C. Porneala *et al.*, "Selective removal of conformal coatings by pulsed ultraviolet lasers," in *Proc. SMTA Int. Conf.*, Sep. 2016, pp. 312–317.

[30] T. Kokubo and H. Takadama, "How useful is SBF in predicting *in vivo* bone bioactivity?" *Biomaterials*, vol. 27, no. 15, pp. 2907–2915, 2006.

Didi She received the B.S. degree in electrical engineering from Southeast University, Nanjing, China, in 2011, and the M.S. degree in microelectronics and solid-state electronics from Peking University, Beijing, China, in 2014. She is currently pursuing the Ph.D. degree in electrical and system engineering with the University of Pennsylvania. Her current research interests focus on the exploration of novel implantable devices for MEMS applications.

Mark G. Allen received the B.A. degree in chemistry, the B.S.E. degree in chemical engineering, and the B.S.E. degree in electrical engineering from the University of Pennsylvania, Philadelphia, and the S.M. and Ph.D. degrees from the Massachusetts Institute of Technology, Cambridge. In 1989, he joined the Faculty of the School of Electrical and Computer Engineering, Georgia Institute of Technology, Atlanta, ultimately holding the rank of Regents' Professor and the J. M. Pettit Professorship in microelectronics, and a joint appointment at the School of Chemical and Biomolecular Engineering. In 2013, he became the Alfred Fitler Moore Professor of electrical and systems engineering and the Scientific Director of the Singh Nanotechnology Center, University of Pennsylvania. He is the Co-Founder of multiple MEMS companies, including Cardiomems, Axion Biosystems, and EnaChip Inc. His research interests are in the development and the application of new micro- and nano-fabrication technologies, and MEMS. He received the IEEE 2016 Daniel P. Noble Award for contributions to research and development, clinical translation, and commercialization of biomedical microsystems. He was the Editor-in-Chief of the *Journal of Micromechanics and Microengineering*, the Co-Chair of the IEEE/ASME MEMS Conference, and the Chair of the 2016 Solid-State Sensors, Actuators, and Microsystems Conference.